The Journal of Engine Research

Journal Homepage: www.engineresearch.ir

DOI:10.22034/ER.2022.697905

Designing Nonlinear Digital Controller for Switching Non Affine Process of Spark Ignition Engine Catalyst Warm-Up

M.R. Homaeinezhad [1*], S. Yaqubi [2], V. Khorrami Rad [3]

[1] [1]*Faculty of Mechanical Engineering, K. N. Toosi University of Technology, Iran, mrhomaeinezhad@kntu.ac.ir*
[2] *Faculty of Mechanical Engineering, K. N. Toosi University of Technology, Iran, sadeq.yaqubi7@gmail.com*
[3] *Faculty of Mechanical Engineering, K. N. Toosi University of Technology, Iran, v.khorrami@email.kntu.ac.ir*
[*] *Corresponding Author*

ARTICLE INFO

Article history:
Received: 22 April 2022
Accepted: 15 June 2022

Keywords:
Digital Engine Control
Switching Process
Spark Ignition (S.I.) Engine
Sliding Mode Control
Robust Control

ABSTRACT

This paper details a new method for model-based discrete sliding mode control of a spark ignition (S.I.) engine cold start considering nonlinear dynamic effects, modeling uncertainty and multiple switched dynamic configurations. Control algorithm deals with stabilization and tracking problems that correspond to crank-shaft velocity, air-to-fuel ratio (AFR) and catalyst temperature in cold start operating mode. To this end, an individual sliding function is assigned to each tracking problem which is subsequently used in construction of associated Lyapunov function. Crank-shaft velocity is regulated using air mass flow rate into intake manifold considering associated dynamic equations describing air mass flow. To ensure precise AFR control, the sliding control model is constructed considering the previously calculated air mass flow rate which leads to nonlinear expressions that are subsequently employed in calculation of appropriate fuel mass flow rate. Stabilization of catalyst temperature is conducted through definition of a virtual control input corresponding to spark angle. As catalyst temperature is described using logarithmic mathematical expressions, additional steps have to be considered to ensure feasibility of control algorithm in various operating conditions. The designed control was numerically applied to validated mathematical model of Toyota 2AZ-FE engine so as to render efficiency and precision of feedback performance.

1) Introduction

Considering the significance of issues pertaining to efficiency, safety and pollution reduction in application of automotive systems, constructing precise control algorithms for engines has been considered of utmost importance in industry for decades [1], [2]. Control of automotive systems inherently involves characteristics such as nonlinearity of governing dynamic, reduction of precision and margins of stability due to existence of modeling uncertainty and hybrid dynamic behaviors. These issues are also among the most significant problems in modern control research. Considering the notable developments attained in aforementioned fields and importance of precise and safe control of automotive machines, proposing an appropriate control model considering robustness to modeling uncertainty in nonlinear switched systems should be considered as an important task.

While traditional control of automotive systems has been conducted using classic linear control techniques or lookup tables, recent developments have also led to application of nonlinear control methods for robust stabilization and tracking problems [3], [4]. Specifically, sliding mode control (SMC) algorithms have been used due to their inherent robustness characteristics and computational efficiency in presence of modeling uncertainty [5], [2]. It has to be noted that conventional SMC methods often feature switching terms which ensure robustness to modeling uncertainty based on continuous investigation of sliding function configuration [6], [7]. resulting in high frequency chattering effects in control inputs. Such control inputs require incorporation of high-speed actuators, and in case chattering effects are not precisely emulated, qualities of tracking precision and closed-loop robust stability do suffer in real-time implementation. As proposed in [8], the aforementioned problems corresponding to modeling uncertainty can be alleviated using adaptive control techniques. However, at times passive sliding control techniques may be beneficial because of lower computational burden which even potentially enable comparable precision since lower calculation burden results in higher-frequency data sampling which in discrete real-time control directly corresponds to tracking precision in presence of modeling uncertainty [10], [9]. Naturally, in case passive SMC techniques are to be incorporated, an efficient algorithm for overcoming chattering effects has to be considered as well. In recent researches such as [9], [10], [11] and Du et al., 2016, generation of control inputs in stabilizing input bounds presented by and generation of admissible inputs without direct effect from switching-based terms have been cited as appropriate methods for overcoming chattering effects in sliding controllers. This philosophy is selected for construction of control scheme in the current research. Incorporation of adaptive control schemes for accurate estimation of system dynamics presented in [12] or use of functions that are less sensitive to alterations in sliding functions as in [13] can be cited as other appropriate schemes for alleviation of chattering effects.

Another significant issue in control of automotive dynamic systems is consideration of multivariable dynamic [14]. As proposed in [15], multivariable controllers are capable of attaining increased tracking precision in comparison with existing single input-single output controllers in case efficient methods for including interaction effects are considered. Additionally, considering the problem of nonlinearity of governing dynamics in real-time applications necessitates construction of the control scheme in discrete-time basis [16], [17]. This arises from the fact that mathematical calculations incorporate in nonlinear controllers cannot be readily implemented using analogue electronic devises and require the use of digital microprocessors. In such systems, calculations are conducted using sampled data in discrete-time basis. Therefore, in case discretization effects are not included in construction of control scheme, closed-loop stability and control performance cannot be guaranteed in real-time applications [18]. Finally, noting that the governing dynamic of automotive systems potentially vary based on operating conditions [8], switched dynamics have to be considered in construction of control model to ensure robust stability in all modes of possible dynamical configurations. In study of amini et. al. [19], the adaptive discrete sliding mode control with application to nonlinear automotive systems was evaluated. In their work, a new formulation of an adaptive second order sliding mode controller is presented for a general class of multi-input multi-output uncertain nonlinear systems. Because in the

conducted study, the type and the number of outputs are supposed to be fixed, the unmanipulated variables might be controlled improperly causing probable instability. In study of amini et.al. [20], bridging the gap between designed and implemented controllers via adaptive robust discrete sliding mode control was evaluated. The main contribution of that study was digital implementation of controller software and considering the uncertainties in the plant's dynamics. The same problem like the previous study [19] still is observed in the conducted study which can be mentioned as the major drawback of research. In study of Kyle Edelberg et. al. [21], design of automotive control systems robust to hardware imprecision was conducted by considering the introduced uncertainty of hardware used for software implementation of engine control system. The designed system was applied to cold start emission control problem of a spark ignition engine. In the proposed control system, the engine was supposed as a single-input single-output system which is opposite to multivariable nature of cold start process of spark ignition engine. In study of amini et. al. [22], discrete sliding controller design with robustness to implementation imprecisions via online uncertainty prediction was designed and implemented. The proposed method suffers mainly from the assumption that supposes the cold start process of a spark ignition engine as a SISO dynamic system. In study of amini et. al [23], handling model and implementation uncertainties via an adaptive discrete sliding mode controller design was introduced. In the mentioned study, no effort was observed so as to solve the problem of controlling spark ignition engine cold start process which is a MIMO system with number of outputs higher than number of inputs.

Considering the addressed problems in digital control of automotive engines, this study proposes a new DSMC technique for MIMO nonlinear switched control of uncertain engine-based systems. The proposed algorithm ensures closed-loop stability and precise tracking in presence of modeling uncertainty based on investigation of sliding functions configuration in various modes of switched dynamic, attaining accurate tracking control of AFR, crankshaft velocity and catalyst temperature which in turn enables the designers to meet the desired standards according to any preset criteria. Compared to existing researches, this work contains the following novelties:

(a) Precise control of engine in automotive system is attained by a robust chattering-free DSMC algorithm considering switched dynamic effects which lead to generation of smooth inputs due to selection of inputs in stabilizing bounds;

(b) The control algorithm is obtained considering nonlinear model-based dynamic at all operating conditions and is not limited to linearization of governing dynamic expressions around a pre-assigned set-point;

(c) An appropriate algorithm for control of catalyst temperature considering nonlinear exponential dynamics is proposed based on suitable virtual input definition and assigning feasible corresponding reference;

(d) In case the feasible virtual input for catalyst temperature is not calculable, a safe-mode controller is proposed based on estimation of system catalyst temperature dynamic with respect to exhaust temperature. As a result, feasible spark angle can be found for all potential configurations of catalyst temperature reference signal;

(e) Control of catalyst temperature is investigated considering switched dynamic, ensuring stabilization of closed-loop algorithm in all potential switched dynamic configurations.

The rest of this paper is organized as follows. Section 2 introduces the considered Toyota 2AZ-FE cold start model for describing engine dynamic. In Section 3, the corresponding DSMC algorithm is constructed investigating the tracking and the stabilization of crank-shaft velocity, AFR and catalyst temperature. Section 4 illustrates performance and efficiency of proposed algorithm for Toyota 2AZ-FE cold start engine. The appendix features nomenclature featuring list of used indices and expressions.

2) Governing Dynamic for Toyota 2AZ-FE Cold Start

In this section, the dynamical model for Toyota 2AZ-FE cold Start engine is expressed. The experimentally validated model of Toyota 2AZ-FE engine was exploited from studies [24]-[25]. This mathematical model is subsequently used to construct the corresponding model-based sliding control algorithm in Section 3. Initially, the continuous-time dynamical model is

presented in this section which is subsequently transformed to discrete-time basis for incorporation in control algorithm.

Considering state variables vector $\underline{\mathbf{x}} \triangleq [x_1, x_2, x_3, x_4, x_5], \underline{\mathbf{x}} \in \mathbb{R}^{5\times 1}$ constituting of air mass in intake manifold (x_1), crankshaft velocity (x_2), fuel mass flow rate (x_3), catalyst temperature (x_4) and exhaust combustion temperature (x_5) alongside with inputs vector $\underline{\mathbf{u}} \triangleq [u_1, u_2, u_3], \underline{\mathbf{u}} \in \mathbb{R}^{3\times 1}$ featuring air mass flow rate into intake manifold (u_1), command mass flow rate of fuel (u_2) and spark timing after top dead position (spark angle) (u_3), continuous-time dynamics are expressed as:

$$\dot{\underline{\mathbf{x}}} = \underline{\mathbf{f}}_j(\underline{\mathbf{x}}, \underline{\mathbf{u}}), j = 1,2 \quad (1)$$

$$\underline{\mathbf{f}}_j(\underline{\mathbf{x}}, \underline{\mathbf{u}}) \triangleq \left[f_1(\underline{\mathbf{x}}, \underline{\mathbf{u}}), f_2(\underline{\mathbf{x}}, \underline{\mathbf{u}}), f_3(\underline{\mathbf{x}}, \underline{\mathbf{u}}), f_{4j}(\underline{\mathbf{x}}, \underline{\mathbf{u}}), f_5(\underline{\mathbf{x}}, \underline{\mathbf{u}})\right]^T, j = 1,2 \quad (2)$$

$\underline{\mathbf{f}}_j(\underline{x}, \underline{u})$ indicates switched governing dynamic where $j \in \mathfrak{E} = \{1,2\}$ expresses switching configurations in the switching set $\mathfrak{E}$. Rewriting expressions used in Amini et al., 2014, Dynamical functions $f_i(\underline{\mathbf{x}}, \underline{\mathbf{u}}), i = 1, \dots, 5$ are defined as:

$$f_1(\underline{\mathbf{x}}, \underline{\mathbf{u}}) \triangleq -p_{1,1}x_1x_2g(\underline{\mathbf{x}}) + u_1 \quad (3)$$

$$f_2(\underline{\mathbf{x}}, \underline{\mathbf{u}}) \triangleq p_{2,1}x_1 + p_{2,2}x_2 + p_{2,3} \quad (4)$$

$$f_3(\underline{\mathbf{x}}, \underline{\mathbf{u}}) \triangleq p_{3,1}x_3 - p_{3,1}u_2 \quad (5)$$

$$f_{4j}(\underline{\mathbf{x}}, \underline{\mathbf{u}}) \triangleq p_{4,1}x_3\left[p_{1,1}x_1x_2g(\underline{\mathbf{x}}) + x_3\right]\left[1 - \exp\left[p_{4,2}\left(\frac{p_{1,1}x_1x_2g(\underline{\mathbf{x}})/(p_{4,4}x_3) - p_{4,5}}{p_{4,3}}\right)^{p_{4,6}}\right]\right] - \exp\left[p_{4,7}\left(\frac{x_4 - p_{4,8}}{p_{4,9}}\right)^{p_{4,10}}\right]\exp\left[p_{4,11}\left(\frac{p_{4,12} - u_3 - p_{4,13}}{p_{4,16,j}\left(\left[p_{1,1}x_1x_2g(\underline{\mathbf{x}})\right]/x_3 + p_{4,14}\right)^{p_{4,15}}} + p_{4,19}(x_5 - x_4) - p_{4,20}(x_4 - p_{4,21})\right), j = 1,2 \quad (6)$$

$$f_5(\underline{\mathbf{x}}, \underline{\mathbf{u}}) \triangleq \frac{x_2}{2\pi}\left[p_{5,2}\cos\left[p_{5,3}\left(\frac{p_{1,1}x_1x_2g(\underline{\mathbf{x}})}{x_3} - p_{5,4}\right)\right] - x_5\right] + \frac{p_{5,1}x_2}{2\pi}\cos\left[p_{5,3}\left(\frac{p_{1,1}x_1x_2g(\underline{\mathbf{x}})}{x_3} - p_{5,4}\right)\right]u_3 \quad (7)$$

$p_{i,j}$s are system parameters contained in the system parameters vector $\underline{\boldsymbol{\Phi}}$ as:

$$\underline{\boldsymbol{\Phi}} \triangleq [p_{1,1}, p_{1,2}, p_{1,3}, p_{1,4}, p_{1,5}, p_{1,6}, p_{1,7}, p_{1,8}, p_{1,9}, p_{1,10}, p_{2,3}, p_{3,1}, p_{4,1}, p_{4,2}, p_{4,3}, p_{4,4}, p_{4,5}, p_{4,6}, p_{4,7}, p_{4,8}, p_{4,9} p_{4,11}, p_{4,12}, p_{4,13}, p_{4,14}, p_{4,15}, p_{4,16,j=1}, p_{4,16,j=2}, p_{4,17} p_{4,19}, p_{4,20}, p_{4,21}, p_{5,1}, p_{5,2}, p_{5,3}, p_{5,4}, p_{h,1}, p_{h,2}]^T \in \boldsymbol{\Phi}_U \subset \mathbb{R}^{24\times 1} \quad (8)$$

$\boldsymbol{\Phi}_U$ is the parametric uncertainty space which is considered as sector-bounded modeling uncertainty in construction of the control algorithm. Dynamical function $g(\underline{\mathbf{x}})$ is defined as:

$$g(\underline{\mathbf{x}}) \triangleq x_1^2(p_{1,2}x_2^2 + p_{1,3}x_2 + p_{1,4}) + x_1(p_{1,5}x_2^2 + p_{1,6}x_2 + p_{1,7}) + p_{1,8}x_2^2 + p_{1,9}x_2 + p_{1,10} \quad (9)$$

In Eq. (2) switching signal is assigned according to configuration of AFR in comparison with stoichiometry factor $p_{4,4}$ as:

$$j = \begin{cases} 1 & \frac{p_{1,1}x_1x_2g(\underline{\mathbf{x}})}{x_3} \geq p_{4,4} \\ 2 & \frac{p_{1,1}x_1x_2g(\underline{\mathbf{x}})}{x_3} < p_{4,4} \end{cases} \quad (10)$$

The switching term is a function of whether AFR is larger than stoichiometric ratio or not. Noting the highly nonlinear dynamic of $f_{4j}(\underline{\mathbf{x}}, \underline{\mathbf{u}})$ featuring logarithmic and exponential terms, virtual control input $u_3^*(t, j)$ is defined which enables us to express governing dynamic as affine to this virtual input in obtaining the control algorithm. This will be expanded on in Section 3.

$$u_3^*(t, j) \triangleq \exp\left[p_{4,11}\left(\frac{p_{4,12} - u_3 - p_{4,13}}{p_{4,16,j}\left(\left[p_{1,1}x_1x_2g(\underline{\mathbf{x}})\right]/x_3 + p_{4,14}\right)^{p_{4,15}}} + \right.\right. \quad (11)$$

3) Construction of Robustly Stabilizing Control Scheme

In this section, the DSMC algorithm for stable tracking control of Toyota 2AZ-FE cold start is presented. As it was discussed, precise control

of automotive engines is considered as a significant task in modern industry because it permits the designers to attain acceptable performance criteria according to standards such as high efficiency and low pollution rate (Tschanz et al., 2013). Attaining such objectives is conducted based on assigning appropriate reference trajectories where precise tracking results in satisfaction of preset goals. In this study, we propose a new method for tracking control of crankshaft velocity x_2, fuel mass flow rate x_3 and catalyst temperature x_4 considering uncertain nonlinear dynamic effects. The proposed control algorithm is designed such that it remains feasible for various operating conditions and reference signals. Therefore, control task is conducted according to nonlinear dynamic models at all operating conditions (rather than assignation of linear expressions corresponding to individual set-points). Additionally, a safe-mode control mode is constructed for stabilization and tracking of catalyst temperature. To these ends, control algorithm for crank-shaft velocity is discussed in Section 3.1, Section 3.2 details the AFR tracking procedure and Section 3.3 discusses the control model for catalyst temperature. The virtual-input based control of catalyst temperature is proposed in Section 3.3.1 and the safe-mode approximation-based control model for catalyst temperature is detailed in Section 3.3.2. Finally, overall description of the control algorithm is presented in Section 3.4.

3.1) Control of Crank-Shaft Velocity

To obtain the DSMC scheme for crank-shaft velocity, governing dynamical expressions Eqs. (3-4) are investigated in order to calculate appropriate rate of air mass flow into intake manifold u_1. To this end, Eqs. (3-4) should be expressed in discrete-time basis. In this study, multi-step Adams-Bashforth method (Hairer et al., 1993) is employed for transformation of continuous-time dynamical expressions to discrete-time basis. Based on sampling period T, the following discrete-time expressions are obtained:

$$\begin{aligned} x_1(k) = x_1(k-1) &+ \frac{3T}{2} f_1\left[\underline{\mathbf{x}}(k-1), \underline{\mathbf{u}}(k-1)\right] \\ &- \frac{T}{2} f_1\left[\underline{\mathbf{x}}(k-2), \underline{\mathbf{u}}(k-2)\right] \\ &= x_1(k-1) \\ &+ \frac{3T}{2}\left[-p_{1,1} x_1(k-1) x_2(k-1) g\left[\underline{\mathbf{x}}(k-1)\right]\right] \\ &- \frac{T}{2}\left[-p_{1,1} x_1(k-2) x_2(k-2) g\left[\underline{\mathbf{x}}(k-2)\right] + u_1(k-2)\right] + \frac{3T}{2} u_1(k-1) \end{aligned} \quad (12)$$

$$\begin{aligned} x_2(k) = x_2(k-1) &+ \frac{3T}{2}\left[p_{2,1} x_1(k-1) + p_{2,2} x_2(k-1) + p_{2,3}\right] \\ &- \frac{T}{2}\left[p_{2,1} x_1(k-2) + p_{2,2} x_2(k-2) + p_{2,3}\right] \end{aligned} \quad (13)$$

where:

$$\begin{aligned} g\left[\underline{\mathbf{x}}(k-1), \boldsymbol{\Phi}\right] = \big[& x_1^2(k-1)\left(p_{1,2} x_2^2(k-1) + p_{1,3} x_2(k-1) + p_{1,4}\right) \\ & + x_1(k-1)\left(p_{1,5} x_2^2(k-1) + p_{1,6} x_2(k-1) + p_{1,7}\right) \\ & + p_{1,8} x_2^2(k-1) + p_{1,9} x_2(k-1) + p_{1,10}\big] \end{aligned} \quad (14)$$

Sliding function $s_1(k)$ corresponding to crank shaft velocity tracking problem is defined as:

$$\begin{aligned} s_1(k) &\triangleq \tilde{x}_2(k) + \lambda_1 \tilde{x}_2(k-1); |\lambda_1| < 1, \tilde{x}_2(k) \\ &\triangleq x_2(k) - x_{2r}(k) \end{aligned} \quad (15)$$

where $x_{2r}(k)$ is the reference signal associated to state $x_2(k)$. λ_1 is sliding function design parameter selected such that convergence of $s_1(k)$ to origin results in elimination of tracking error. From z-transform analysis of Eq. (13), it is obtained that admissible region for sliding function design parameter is $|\lambda_1| < 1$. To calculate the required rate of air mass flow into intake manifold u_1, the candidate Lyapunov function (CLF) $V_1(k)$ is assigned.

$$V_1(k) \triangleq s_1^2(k) \quad (16)$$

The condition of monotonic decrease of CLF leads to:

$$\begin{aligned} V_1(k+1) - V_1(k) < 0 \Rightarrow s_1^2(k+1) - s_1^2(k) &< 0 \Longrightarrow -|s_1(k)| \\ &< s_1(k+1) < +|s_1(k)| \end{aligned} \quad (17)$$

To obtain sliding function at current sample as $s_1(k)$, from Eq. (15) and Eq. (4) it follows that:

$$\begin{aligned} s_1(k) \triangleq\ & x_2(k) - x_{2r}(k) + \lambda_1 \tilde{x}_2(k-1) \\ =\ & x_2(k-1) \\ & + \frac{3T}{2}\left[p_{2,1}x_1(k-1)\right. \\ & \left. + p_{2,2}x_2(k-1) + p_{2,3}\right] \\ & - \frac{T}{2}\left[p_{2,1}x_1(k-2)\right. \\ & \left. + p_{2,2}x_2(k-2) + p_{2,3}\right] \\ & - x_{2r}(k) + \lambda_1 \tilde{x}_2(k-1) \end{aligned} \quad (18)$$

Subsequent sample sliding function $s_1(k+1)$ can now be calculated by shifting the expressions of Eq. (18) up one sample and substituting $x_1(k)$ from Eq. (2).

$$s_1(k+1) = \xi_1[k, \boldsymbol{\Phi}] + b_1 u_1(k-1) \quad (19)$$

$$\begin{aligned} \xi_1[k, \boldsymbol{\Phi}] \triangleq\ & \left(1 + \lambda_1 + \frac{3T}{2}p_{2,2}\right)\left[x_2(k-1)\right. \\ & + \frac{3T}{2}\left[p_{2,1}x_1(k-1)\right. \\ & \left. + p_{2,2}x_2(k-1) + p_{2,3}\right] \\ & - \frac{T}{2}\left[p_{2,1}x_1(k-2)\right. \\ & \left. \left. + p_{2,2}x_2(k-2) + p_{2,3}\right]\right] \\ & + \frac{3T}{2}\left[p_{2,1}\left[x_1(k-1)\right.\right. \\ & + \frac{3T}{2}\left[-p_{1,1}x_1(k-1)x_2(k\right. \\ & \left.\left. - 1)g\left[\underline{\mathbf{x}}(k-1)\right]\right] \\ & - \frac{T}{2}\left[-p_{1,1}x_1(k-2)x_2(k\right. \\ & \left. - 2)g\left[\underline{\mathbf{x}}(k-2)\right] + u_1(k\right. \\ & \left.\left. - 2)\right]\right] + p_{2,3}\Big] \\ & - \frac{T}{2}\left[p_{2,1}x_1(k-1)\right. \\ & \left. + p_{2,2}x_2(k-1) + p_{2,3}\right] \\ & - x_{2r}(k+1) - \lambda_1 x_{2r}(k) \end{aligned} \quad (20)$$

$$b_1 \triangleq \left(\frac{3T}{2}\right)^2 \quad (21)$$

Now, the term $\xi_1[k, \boldsymbol{\Phi}]$ featuring dynamical expressions and reference signal terms can be readily calculated based on existing measurements at time sample $k-1$. The control input gain b_1 corresponding to this control stage is constant and is solely a function of sampling period. Substituting Eq. (19) in Eq. (17), stabilization bounds are obtained as:

$$\begin{aligned} -|s_1(k)| <\ & \xi_1[k, \boldsymbol{\Phi}] + b_1 u_1(k-1) \\ <\ & +|s_1(k)| \end{aligned} \quad (22)$$

To ensure robustness of the control scheme to modeling uncertainty, boundary values of sides of Eq. (22) should be calculated over bounded uncertainty space $\boldsymbol{\Phi_U}$ [2].

$$\begin{aligned} \mathrm{Sup}\left[-\xi_1[k, \boldsymbol{\Phi}]\right]_{\boldsymbol{\Phi_U}} - |s_1(k)| <\ & u_1(k-1) \\ <\ & +|s_1(k)| \\ & - \mathrm{Inf}\left[-\xi_1[k, \boldsymbol{\Phi}]\right]_{\boldsymbol{\Phi_U}} \end{aligned} \quad (23)$$

In Eq. (23) $\mathrm{Sup}[-]_{\boldsymbol{\Phi_U}}$ and $\mathrm{Inf}[-]_{\boldsymbol{\Phi_U}}$ respectively express supremum and infimum of bracketed term over bounded uncertainty space $\boldsymbol{\Phi_U}$.

Remark 1. For feasibility of convex inequality expressed in Eq. (23), it should be obtained that $\mathrm{Sup}\left[-\xi_1[k, \boldsymbol{\Phi}]\right]_{\boldsymbol{\Phi_U}} - |s_1(k)| < +|s_1(k)| - \mathrm{Inf}\left[-\xi_1[k, \boldsymbol{\Phi}]\right]_{\boldsymbol{\Phi_U}}$. Then, minimum admissible width of sliding layer $|s_1(k)|$ is equivalent to $\rho_1(k) = \frac{1}{2}\left[\mathrm{Sup}\left[-\xi_1[k, \boldsymbol{\Phi}]\right]_{\boldsymbol{\Phi_U}} - \mathrm{Inf}\left[-\xi_1[k, \boldsymbol{\Phi}]\right]_{\boldsymbol{\Phi_U}}\right]$ which is a function of sampling period $\mathcal{O}(T)$ in discrete-time basis. In case $|s_1(k)| < \rho_1(k)$, $\rho_1(k)$ is used in place of $|s_1(k)|$ in Eq. (23).

Finally, based on assigning a control bounds proximity factor $\alpha_1(k) \epsilon (0,1)$, control input $u_1(k-1)$ is calculated.

$$\begin{aligned} u_1(k-1) = & [1 - \alpha_1(k)]\left[\mathrm{Sup}\left[-\xi_1[k, \boldsymbol{\Phi}]\right]_{\boldsymbol{\Phi_U}}\right. \\ & \left. - |s_1(k)|\right] \\ & + \alpha_1(k)\left[+|s_1(k)|\right. \\ & \left. + \mathrm{Inf}\left[-\xi_1[k, \boldsymbol{\Phi}]\right]_{\boldsymbol{\Phi_U}}\right], 0 \\ & < \alpha_1(k) < 1 \end{aligned} \quad (24)$$

Since selection of control input $u_1(k-1)$ according to Eq. (20) results in reduction of CLF $V_1(k)$ with respect to Eq. (17), asymptotic stability and appropriate tracking response of the closed-loop system is guaranteed. Furthermore, since control input bounds are constructed according to boundary values of modeling uncertainty according to Eq. (23), the control algorithm is robust to all configurations of parametric uncertainty bounded in $\boldsymbol{\Phi_U}$. It should be also noted that since control inputs are not directly dependent on switching terms, the effects of high-frequency chattering in generated control input do not occur.

3.2) AFR Control

In this section, the second part of DSMC scheme is proposed which involves model-based nonlinear tracking control of AFR. In most conducted studies, AFR tracking is conducted based on linearization of nonlinear dynamical expressions revolving around a set-point. However, obtaining more general control scheme ensuring precise tracking response for all admissible regions necessitates incorporation of nonlinear dynamical effects in

control algorithm. However, it has to be noted that AFR in itself is not a system state according to Eqs. (3-7), therefore the output $y(k-1)$ is assigned to AFR.

$$y(k-1) \triangleq \frac{p_{1,1}x_1(k-1)x_2(k-1)g[\underline{\mathbf{x}}(k-1)]}{x_3(k-1)} \quad (25)$$

The corresponding tracking problem to AFR is investigated based on the sliding function $s_2(k)$ and according to viable sliding function design parameter λ_2 as:

$$s_2(k) \triangleq \tilde{y}(k-1) + \lambda_2\tilde{y}(k-2); |\lambda_2| < 1, \tilde{y}(k) \triangleq y(k) - y_r(k) \quad (26)$$

$y_r(k)$ indicates the assigned AFR reference signal. Similar to Section 3.1, the sliding function at subsequent sample should be calculated according to governing dynamical expression Eqs. (3-5).

$$\begin{aligned} s_2(k+1) &= \tilde{y}(k) + \lambda_2\tilde{y}(k-1) \\ &= y(k) - y_r(k) + \lambda_2\tilde{y}(k-1) \\ &= \frac{p_{1,1}x_1(k)x_2(k)g[\underline{\mathbf{x}}(k)]}{x_3(k)} - y_r(k) \\ &+ \lambda_2\tilde{y}(k-1) \\ &= \left(p_{1,1}x_1(k)x_2(k)g[\underline{\mathbf{x}}(k),\boldsymbol{\Phi}]\right) \\ &/\left(x_3(k-1)\right. \\ &+ \frac{3T}{2}\left[p_{3,1}x_3(k-1) - p_{3,1}u_2(k-1)\right] \\ &- \left.\frac{T}{2}\left[p_{3,1}x_3(k-2) - p_{3,1}u_2(k-2)\right]\right) \\ &- y_r(k) + \lambda_2\tilde{y}(k-1) \end{aligned} \quad (27)$$

Discrete-time dynamical term $g[\underline{\mathbf{x}}(k),\boldsymbol{\Phi}]$ is defined as:

$$\begin{aligned} g[\underline{\mathbf{x}}(k),\boldsymbol{\Phi}] \triangleq \big[&x_1^2(k)\left[p_{1,2}x_2^2(k) + p_{1,3}x_2(k) + p_{1,4}\right] \\ &+ x_1(k)\left[p_{1,5}x_2^2(k) + p_{1,6}x_2(k) + p_{1,7}\right] \\ &+ p_{1,8}x_2^2(k) + p_{1,9}x_2(k) + p_{1,10}\big] = g[\underline{\mathbf{x}}(k),\boldsymbol{\Phi}] \end{aligned} \quad (28)$$

Remark 2. Note that in Eq. (28), the terms $x_1(k)$, $x_2(k)$ and $g[\underline{\mathbf{x}}(k),\boldsymbol{\Phi}]$ are readily calculable according to Eqs. (3-4) as $u_1(k-1)$ has been calculated in Eq. (24). Then, substituting $u_1(k-1)$ in Eqs. (12-13), the term $x_1(k)x_2(k)g[\underline{\mathbf{x}}(k),\boldsymbol{\Phi}]$ is computed. Now, it can be observed that command mass flow rate of fuel $u_2(k-1)$ has to be calculated as control input corresponding to this control stage.

To obtain appropriate control input, the CLF $V_2(k)$ is assigned.

$$V_2(k) \triangleq s_2^2(k) \quad (29)$$

The condition of monotonic reduction of CLF leads to:

$$\begin{aligned} V_2(k+1) - V_2(k) < 0 &\Rightarrow s_2^2(k+1) - s_2^2(k) \\ &< 0 \Longrightarrow -|s_2(k)| \\ &< s_2(k+1) < +|s_2(k)| \end{aligned} \quad (30)$$

Similar to Section 3.1, to ensure robustness in presence of modeling uncertainty, Eq. (30) is rewritten according to worst-case configuration of system uncertainty as:

$$\begin{aligned} \mathrm{Sup}\left[q_2^{(L)}[k,\boldsymbol{\Phi}]\right]_{\boldsymbol{\Phi_U}} &< u_2(k-1) \\ &< Inf\left[q_2^{(H)}[k,\boldsymbol{\Phi}]\right]_{\boldsymbol{\Phi_U}} \end{aligned} \quad (31)$$

where:

$$\begin{aligned} &q_2^{(L)}[k,\boldsymbol{\Phi}] \\ &\triangleq p_{3,1}^{-1}\Bigg[-p_{3,1}x_3(k-1) \\ &+ \frac{2}{3T}\Bigg[-x_3(k-1) \\ &+ \frac{T}{2}\big[p_{3,1}x_3(k-2) \\ &- p_{3,1}u_2(k \\ &- 2)\big]\frac{p_{1,1}x_1(k)x_2(k)g[\underline{\mathbf{x}}(k),\boldsymbol{\Phi}]}{y_r(k) - \lambda_2\tilde{y}(k-1) - |s_2(k)|}\Bigg]\Bigg]; \\ &q_2^{(H)}[k,\boldsymbol{\Phi}] \\ &\triangleq p_{3,1}^{-1}\Bigg[\frac{2}{3T}\Bigg[\frac{p_{1,1}x_1(k)x_2(k)g[\underline{\mathbf{x}}(k),\boldsymbol{\Phi}]}{+|s_2(k)| + y_r(k) - \lambda_2\tilde{y}(k-1)} \\ &+ \frac{T}{2}\left[p_{3,1}x_3(k-2) - p_{3,1}u_2(k-2)\right] \\ &- x_3(k-1)\Bigg] - p_{3,1}x_3(k-1)\Bigg] \end{aligned} \quad (32)$$

Then, using input bounds proximity factor $\alpha_2(k) \in (0,1)$, control input $u_2(k-1)$ is generated as:

$$\begin{aligned} &u_2(k-1) \\ &= [1-\alpha_2(k)]\mathrm{Sup}\left[q_2^{(L)}[k,\boldsymbol{\Phi}]\right]_{\boldsymbol{\Phi_U}} \\ &+ \alpha_2(k)\mathrm{Inf}\left[q_2^{(H)}[k,\boldsymbol{\Phi}]\right]_{\boldsymbol{\Phi_U}}, 0 < \alpha_2(k) < 1 \end{aligned} \quad (33)$$

As selection of $u_2(k-1)$ according to Eq. (29) results in monotonic decrease of CLF $V_2(k)$, then corresponding closed-loop system at this stage is asymptotically stable for all potential configurations of modeling uncertainty bounded in $\boldsymbol{\Phi_U}$.

3.3) Catalyst Temperature Control

This section details tracking control for catalyst temperature considering nonlinear dynamic effects. It was noted that this section of system dynamic Eq. (6) is not affine to spark timing after top dead position of piston u_3 therefore a virtual control input $u_3^*(t,j)$ was assigned in Eq. (11). As this virtual input is expressed as a logarithmic function, the actual input may not

be feasible at al all times. To address this issue, catalyst temperature control is conducted in a dual-mode basis. Specifically, if virtual control is viable, then precise-mode control inputs can be calculated according to Section 3.3.1. However, if this is not feasible, we propose an alternate safe-mode control strategy in Section 3.3.2 based on approximation of catalyst temperature dynamic with respect to exhaust temperature.

3.4) Precise-Mode Control of Catalyst Temperature

In discrete-time basis, governing dynamics corresponding to catalyst temperature are expressed as:

$$x_{4j}(k) = h_j(k, \boldsymbol{\Phi}) + \sigma_j(k, \boldsymbol{\Phi}) u_3^*(k-1, j) \quad (34)$$

In Eq. (34), $x_{4j}(k)$ indicates catalyst temperature in case j'th switched mode is active according to Eq. (10). Dynamic term $h_j(k, \boldsymbol{\Phi})$ is defined as:

$$\begin{aligned} & h_j(k, \boldsymbol{\Phi}) \\ & \triangleq x_{4j}(k-1) \\ & + \frac{3T}{2}\left[p_{4,19}\left[x_5(k-1) - x_{4j}(k-1)\right] - p_{4,20}\left[x_{4j}(k-1) - p_{4,21}\right]\right] \\ & - \frac{T}{2}\left\{ p_{4,1} x_3(k-2)\left[p_{1,1} x_1(k-2) x_2(k-2) g\left[\underline{\mathbf{x}}(k-2)\right] + x_3(k-2)\right]\left[1 - \exp\left[p_{4,2}\left(\frac{p_{1,1} x_1(k-2) x_2(k-2) g\left[\underline{\mathbf{x}}(k-2)\right]}{p_{4,3}}\right)\right]\right] \right. \\ & \left. \exp\left[p_{4,7}\left(\frac{x_{4j}(k-2) - p_{4,8}}{p_{4,9}}\right)^{p_{4,10}}\right] u_3^*(k-2, j) + p_{4,19}\left[x_5(k-2) - x_{4j}(k-2)\right] - p_{4,20}\left[x_{4j}(k-2) - p_{4,21}\right] \right\} \end{aligned} \quad (35)$$

Control input gain $\sigma_j(k, \boldsymbol{\Phi})$ for virtual input $u_3^*(k-1, j)$ is expressed in Eq. (36).

$$\begin{aligned}\sigma_j(k,\boldsymbol{\Phi}) &\triangleq \frac{3T}{2}p_{4,1}x_3(k-1)\left[p_{1,1}x_1(k-1)x_2(k-1)g\left[\underline{\mathbf{x}}(k-1)\right]+x_3(k-1)\right]\left|1\right. \\ &\quad -\exp\left[p_{4,2}\left(\left.\frac{p_{1,1}x_1(k-1)x_2(k-1)g\left[\underline{\mathbf{x}}(k-1)\right]}{p_{4,3}}\right)\right.\right. \\ &\quad \left.\left.-\exp\left[p_{4,7}\left(\frac{x_{4j}(k-1)-p_{4,8}}{p_{4,9}}\right)^{p_{4,10}}\right]\right]\end{aligned} \quad (36)$$

Then, sliding function corresponding to the catalyst temperature tracking problem $s_{3,j}(k)$ is defined using design parameter λ_3.

$$\begin{aligned}s_{3,j}(k) &\triangleq \tilde{x}_{4,j}(k-1)+\lambda_3\tilde{x}_{4,j}(k-2);|\lambda_3| \\ &< 1,\tilde{x}_{4,1}(k) \\ &\triangleq x_{4,1}(k)-x_{4r}(k);j=1,2\end{aligned} \quad (37)$$

At subsequent sample, sliding function is calculated as:

$$\begin{aligned}s_{3,j}(k+1) &= \tilde{x}_{4,j}(k)+\lambda_3\tilde{x}_{4,j}(k-1) \\ &= h_j(k,\boldsymbol{\Phi}) \\ &\quad +\sigma_j(k,\boldsymbol{\Phi})u_3^*(k-1,j) \\ &\quad -x_{4r}(k)+\lambda_3\tilde{x}_{4,j}(k-1);\end{aligned} \quad (38)$$

$$\zeta_j(k,\boldsymbol{\Phi}) \triangleq h_j(k,\boldsymbol{\Phi})-x_{4r}(k)+\lambda_3\tilde{x}_{4,j}(k-1)$$

Now, the CLF $V_3(k)$ is assigned.

$$V_3(k) \triangleq s_{3,j}^2(k) \quad (39)$$

Monotonic decrease of CLF is investigated as:

$$\begin{aligned}V_3(k+1)-V_3(k) &< 0 \\ &\Rightarrow s_{3,j}^2(k+1)-s_{3,j}^2(k)<0 \\ &\Longrightarrow -\left|s_{3,j}(k)\right| < s_{3,j}(k+1) \\ &< +\left|s_{3,j}(k)\right|\end{aligned} \quad (40)$$

It should be noted that governing dynamics corresponding to this section is switched depending on value of AFR with respect to stoichiometric ratio, therefore the dwell-time condition of switching signal for stability of closed-loop system should be calculated. To this end, Eq. (40) is tightened using finite-time convergence factor $\mu \in (0,1)$.

$$-\mu\left|s_{3,j}(k)\right| < s_{3,j}(k+1) < +\mu\left|s_{3,j}(k)\right| \quad (41)$$

Substituting Eq. (38) into Eq. (41), it is obtained that:

$$\begin{aligned}-\mu\left|s_{3,j}(k)\right| &< \zeta_j(k,\boldsymbol{\Phi})+\sigma_j(k,\boldsymbol{\Phi})u_3^*(k-1,j) \\ &< +\mu\left|s_{3,j}(k)\right|\end{aligned} \quad (42)$$

Robust control input can be generated similar to Sections 3.1 and 3.2 using worst-case disturbance configuration as:

$$\begin{aligned}&\mathrm{Sup}\left[\frac{-\zeta_j(k,\boldsymbol{\Phi})-\mu\left|s_{3,j}(k)\right|}{\sigma_j(k,\boldsymbol{\Phi})}\right]_{\boldsymbol{\Phi_U}} < u_3^*(k-1,j) \\ &< Inf\left[\frac{+\mu\left|s_{3,j}(k)\right|-\zeta_j(k,\boldsymbol{\Phi})}{\sigma_j(k,\boldsymbol{\Phi})}\right]_{\boldsymbol{\Phi_U}}\end{aligned} \quad (43)$$

Now, virtual control input can be generated using input bounds proximity factor $\alpha_3(k)$.

$$\begin{aligned}u_3^*(k-1,j) &= [1-\alpha_3(k)]\mathrm{Sup}\left[\frac{-\zeta_j(k,\boldsymbol{\Phi})-\mu\left|s_{3,j}(k)\right|}{\sigma_j(k,\boldsymbol{\Phi})}\right]_{\boldsymbol{\Phi_U}} \\ &\quad +\alpha_3(k)\mathrm{Inf}\left[\frac{+\mu\left|s_{3,j}(k)\right|-\zeta_j(k,\boldsymbol{\Phi})}{\sigma_j(k,\boldsymbol{\Phi})}\right]_{\boldsymbol{\Phi_U}},0 \\ &< \alpha_3(k)<1\end{aligned} \quad (44)$$

Finally, actual control input $u_3(k)$ is calculated according to Eq. (11) and Eq. (44) given positive $u_3^*(k-1,j)$ can be found with respect to assigned reference signal.

$$\begin{aligned}u_{3f}(k-1) &= p_{4,12}-p_{4,13} \\ &\quad -\left[p_{4,16,j}\left(\left.\left[p_{1,1}x_1(k-1)x_2(k-1)g\left[\underline{\mathbf{x}}(k-1)\right]\right]\right/_{\mathrm{X}}+p_{4,14}\right)^{p_{4,15}}+p_{4,17}\right]^{p_{4,18}}\sqrt{\frac{\ln[u_3^*(k-1,j)]}{p_{4,11}}}\end{aligned} \quad (45)$$

Remark 3 (switching signal conditions). For viability of Eq. (43), minimum width of sliding layer is expressed as $\rho_3 = \frac{1}{2\mu}\left[\mathrm{Sup}\left[\frac{-\zeta_j(k,\boldsymbol{\Phi})}{\sigma_j(k,\boldsymbol{\Phi})}\right]_{\boldsymbol{\Phi_U}} - \mathrm{Inf}\left[\frac{+\mu\left|s_{3,j}(k)\right|}{\sigma_j(k,\boldsymbol{\Phi})}\right]_{\boldsymbol{\Phi_U}}\right]$. On the other hand, from Eq. (41), it is obtained that $\left|s_{3,j}(k+1)\right| < \mu\left|s_{3,j}(k)\right|$ in case asymptotically stabilizing input Eq. (45) is assigned. From this, it is resulted that:

$$\begin{aligned}\left|s_{3,j}(1)\right| < \mu\left|s_{3,j}(0)\right| &\Rightarrow \left|s_{3,j}(2)\right| < \mu\left|s_{3,j}(1)\right| \\ &< \mu^2\left|s_{3,j}(0)\right| \Rightarrow \cdots \\ &\Rightarrow \left|s_{3,j}(k)\right| << \mu^k\left|s_{3,j}(0)\right|\end{aligned} \quad (46)$$

Solving $\mu^k\left|s_{3,j}(0)\right| = \rho_3$, the number of samples required for converging to the sliding layer is calculated as $N = \log_\mu\left[\frac{\rho_3}{\left|s_{3,j}(0)\right|}\right]$. Naturally, if the number of samples between alterations in switching signal is smaller than N, convergence cannot be guaranteed. Therefore, N is considered as minimum admissible dwell-time of switching signal.

3.4.1) Safe-Mode Control of Catalyst Temperature

Note that $u_3(k)$ cannot be calculated from $u_3^*(k-1,j)$ if $u_3^*(k-1,j)$ is non-positive according to Eq. (46). Based on this, incorporation of a safe-mode control scheme for such cases is necessary. To obtain the safe-mode control scheme, it is noted that catalyst temperature can be estimated as a function of exhaust temperature $x_5(k-1)$ using Laplace operator $\mathcal{L}$ as:

$$\mathcal{L}\left[\frac{x_4}{x_5}\right] = K_1\frac{\omega_0}{s+\omega_0} \Rightarrow x_5 = \frac{\dot{x}_4 + \omega_0 x_4}{K_1\omega_0} \quad (47)$$

K_1 and ω_0 are estimated parameters that describe catalyst temperature dynamic with respect to exhaust temperature based on available experimental data. Noting Eq. (47), x_4 can be controlled in case corresponding reference x_{5r} for exhaust temperature is assigned. This is expressed as:

$$x_{5r}(k-1) \triangleq \frac{\frac{x_4(k-1)-x_4(k-2)}{T} + \omega_0 x_4(k-1)}{K_1\omega_0} \quad (48)$$

Now, to obtain the modified control scheme, discrete-time expression of exhaust temperature is written according to Eq. (7) as

$$x_5(k) = \eta(k,\boldsymbol{\Phi}) + \sigma_5(k,\boldsymbol{\Phi})u_3(k-1) \quad (49)$$

where:

$$\begin{aligned}\eta(k,\boldsymbol{\Phi}) &\triangleq x_5(k-1) \\ &+ \frac{3T}{2}\left[\frac{x_2(k-1)}{2\pi}\left[p_{5,2}\cos\left[p_{5,3}\left(\frac{p_{1,1}x_1(k-1)x_2(k-}{x_3(k-}\right.\right.\right. \\ &\left.\left.\left.- p_{5,4}\right)\right] - x_5(k-1)\right]\right] \\ &- \frac{T}{2}\left[\frac{x_2(k-2)}{2\pi}\left[p_{5,2}\cos\left[p_{5,3}\left(\frac{p_{1,1}x_1(k-2)x_2(k-}{x_3(k-2}\right.\right.\right. \\ &\left.\left.\left.- p_{5,4}\right)\right] - x_5(k-2)\right] \\ &+ \frac{p_{5,1}x_2(k-2)}{2\pi}\cos\left[p_{5,3}\left(\frac{p_{1,1}x_1(k-2)x_2(k-2)g\right|}{x_3(k-2)}\right.\right. \\ &\left.\left.- p_{5,4}\right)\right]u_3(k-2)\Bigg]\end{aligned} \quad (50)$$

$$\begin{aligned}\sigma_5(k,\boldsymbol{\Phi}) &\triangleq \frac{3T}{2}\frac{p_{5,1}x_2(k-1)}{2\pi}\cos\left[p_{5,3}\left(\frac{p_{1,1}x_1(k-1)x_2(k-1}{x_3(k-1}\right.\right. \\ &\left.\left.- p_{5,4}\right)\right]\end{aligned} \quad (51)$$

Sliding function $s_4(k)$ corresponding to this control mode is then assigned.

$$\begin{aligned}s_4(k) &\triangleq \tilde{x}_5(k-1) + \lambda_4\tilde{x}_5(k-2); |\lambda_4| \\ &< 1, \tilde{x}_5(k) \\ &\triangleq x_5(k) - x_{5r}(k)\end{aligned} \quad (52)$$

Subsequent sample sliding function is calculated based on substituting Eq. (49) in Eq. (52).

$$\begin{aligned}s_4(k+1) &= x_5(k) - x_{5r}(k) + \lambda_4\tilde{x}_5(k-2) \\ &= \eta(k,\boldsymbol{\Phi}) + \sigma_5(k,\boldsymbol{\Phi})u_3(k \\ &- 1) - x_{5r}(k) \\ &+ \lambda_4\tilde{x}_5(k-2)\end{aligned} \quad (53)$$

Then, assigning the CLF $V_4(k)$ and investigating monotonic decrease condition, it is obtained that:

$$\begin{aligned}V_4(k) \triangleq s_4^2(k) &\Rightarrow V_4(k+1) - V_4(k) < 0 \\ &\Rightarrow s_4^2(k+1) - s_4^2(k) < 0 \\ &\Longrightarrow -|s_4(k)| < s_4(k+1) \\ &< +|s_4(k)|\end{aligned} \quad (54)$$

Substituting Eq. (53) into Eq. (54) and tightening it using convergence factor μ according to Eq. (42), stabilizing bounds are obtained as:

$$\begin{aligned}-\mu|s_4(k)| < \eta(k,\boldsymbol{\Phi}) &+ \sigma_5(k,\boldsymbol{\Phi})u_3(k-1) \\ &- x_{5r}(k) + \lambda_4\tilde{x}_5(k-2) \\ &< +\mu|s_4(k)|\end{aligned} \quad (55)$$

Calculating boundary values for robustness is conducted next.

$$\begin{aligned}&\mathrm{Sup}\left[\frac{-\lambda_4\tilde{x}_5(k-2) + x_{5r}(k) - \eta(k,\boldsymbol{\Phi}) - |s_4(k)|}{\sigma_5(k,\boldsymbol{\Phi})}\right] \\ &< u_3(k-1) \\ &< Inf\left[\frac{+|s_4(k)| - \eta(k,\boldsymbol{\Phi}) + x_{5r}(k) - \lambda_4\tilde{x}_5(k-2}{\sigma_5(k,\boldsymbol{\Phi})}\right.\end{aligned} \quad (56)$$

Finally, safe mode control input is calculated based on proximity factor $\alpha_4(k)$.

$$\begin{aligned}u_{3e}(k-1) &\triangleq [1 \\ &- \alpha_4(k)]\mathrm{Sup}\left[\frac{-\lambda_4\tilde{x}_5(k-2) + x_{5r}(k) - \eta(k,\boldsymbol{\Phi}) - |s_4(k)|}{\sigma_5(k,\boldsymbol{\Phi})}\right]_{\boldsymbol{\Phi_U}} \\ &+ \alpha_4(k)\mathrm{Inf}\left[\frac{+|s_4(k)| - \eta(k,\boldsymbol{\Phi}) + x_{5r}(k) - \lambda_4\tilde{x}_5(k-2)}{\sigma_5(k,\boldsymbol{\Phi})}\right]_{\boldsymbol{\Phi_U}}, 0 \\ &< \alpha_4(k) < 1\end{aligned} \quad (57)$$

3.5) DSMC Control for Toyota 2AZ-FE Cold Start (DCTCS)

In Sections 3.1-3.3, the control schemes for tracking problems corresponding to crank-shaft velocity, AFR and catalyst temperature have been presented. Using nonlinear model-based uncertain expressions, control algorithms associated with stabilization and tracking problems were presented considering general sector-bounded modeling uncertainties and noting switched catalyst temperature dynamic. Additionally, a safe-mode control algorithm for increased feasibility in Section 3.3.2 was presented. Combined, the control algorithm is

capable of precise reference tracking and stabilization corresponding states and outputs in Toyota 2AZ-FE cold start engine considering nonlinear dynamic effects for all operating conditions (since linearization around a set-point was not employed). Summarizing the detailed procedure, the proposed DCTCS scheme can be described in block-diagram format in Figure 1.

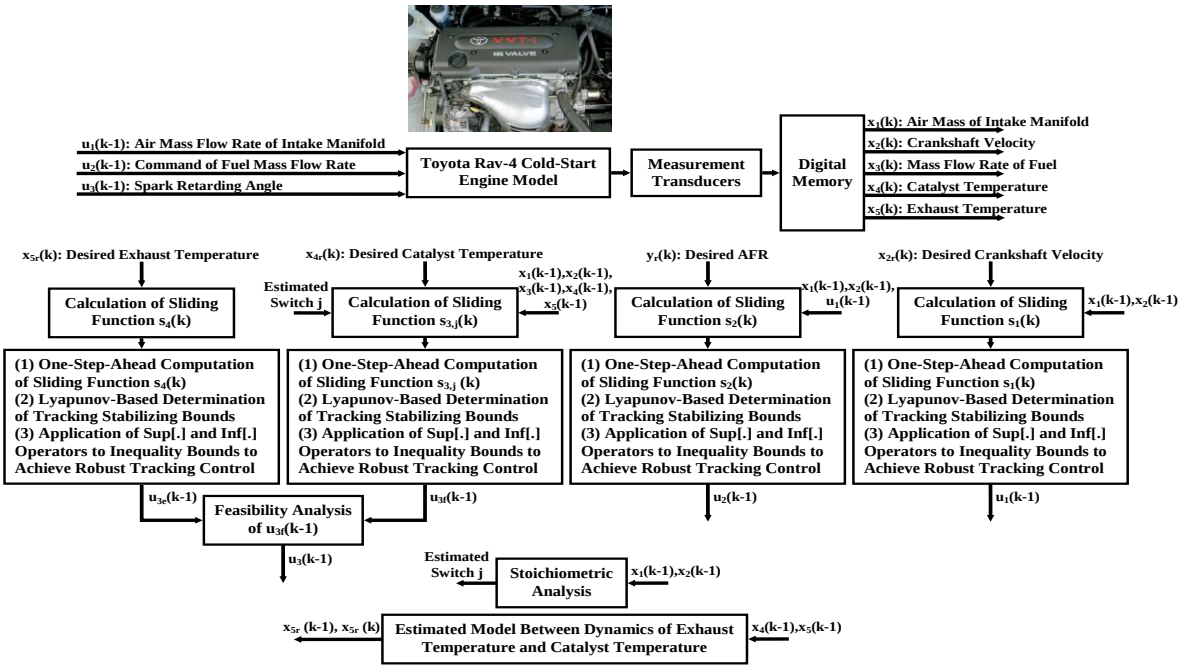

Figure 1: Schematic description of DCTCS algorithm

4) Numerical illustrations

In this section, the performance of DCTCS algorithm is investigated using numerical simulations. To this end, the dynamical system model for Toyota 2AZ-FE Cold Start expressed in Section 2 is considered for employing the closed-loop control algorithm presented in Section 3. As it was detailed, the robust stabilization and reference tracking task is conducted considering nonlinear dynamical effects, modeling uncertainty and switched dynamic variations. Furthermore, as the corresponding control inputs are generated without incorporation of direct switching terms, high-frequency chattering effects are eliminated from the system response. To this end, governing dynamical Eqs. (3-7) are considered based on experimentally verified system parameters (described in [24]) contained in Eq. (8) as:

$$
\begin{aligned}
&p_{1,1} = 0.0254, \quad p_{1,2} = -0.1636, \\
&p_{1,3} = -7.093, \quad p_{1,4} = -1750, \quad p_{1,5} = \\
&0.0029, \quad p_{1,6} = -0.4033, \quad p_{1,7} = 85.38, \\
&p_{1,8} = -1.06e-5, \quad p_{1,9} = 0.0021, \\
&p_{1,10} = 0.2719, \quad p_{2,1} = 206327.372765, \\
&p_{2,2} = -2.751032, \\
&p_{2,3} = -687.757909, p_{3,1} = -16.6667, \\
&p_{4,1} = 0.015701, \quad p_{4,2} = -5, \quad p_{4,3} = 0.3, \\
&p_{4,4} = 14.70, \quad p_{4,5} = 0.7, \quad p_{4,6} = 15, \\
&p_{4,7} = -0.2, \quad p_{4,8} = 30, \quad p_{4,9} = 150, \\
&p_{4,10} = 5, \quad p_{4,11} = -2, \quad p\_4,12 = 110, \\
&p_{4,13} = 10, \quad p_{4,14} = -16.20, \quad p_{4,15} = \\
&2, p_{4,16,1} = 0.1, \quad p_{4,16,2} = 0.4, \quad p_{4,17} = 80, \\
&p_{4,18} = 5, p_{4,19} = 0.0128, p_{4,20} = 5.136e-4, \quad p_{4,21} = 27, \quad p_{5,1} = 7.5, \quad p_{5,2} = 600, \\
&p_{5,3} = 0.13, \quad p_{5,4} = 13.5, \quad p_h, 1 = 0.98, \\
&p_h, 2 = 0.8889
\end{aligned}
\tag{58}
$$

Sliding function design parameters λ_1, λ_2 and λ_3 are set to 0.1. Input bounds proximity factors α_1 and α_2 are set to 0.5. This results in fast convergence to corresponding reference signals for crank-shaft velocity and AFR. Proximity factors α_3 and α_4 are set to 0.95. Convergence factor $\mu = 0.995$ is assigned. This results in slower convergence to associated sliding sets, which is selected as such in order to be

compatible with slower dynamical variations corresponding to catalyst temperature dynamic. We consider -5% additive uncertainty for parameters $p_{1,i}$ corresponding to Eq. (3), 25% additive uncertainty for parameters $p_{2,i}$ corresponding to Eq. (4), 25% additive uncertainty for parameters $p_{3,i}$ corresponding to Eq. (5), 5% additive uncertainty for parameters $p_{4,i}$ corresponding to Eq. (6) and 10% additive uncertainty for parameters $p_{5,i}$ corresponding to Eq. (7). Sampling period $T = 0.005[s]$ is selected which is attainable using available sensors and actuators. Initially, harmonic reference signals generated around admissible initial constants as expressed in Eq. (54) are considered for initial simulation of the closed-loop system.

$$x_{2r}(t) = 130 + 10\cos 1.0t \ [rad/s]$$
$$y(t) = 14 + 0.5\cos 0.2t \quad (59)$$
$$x_{4r}(t) = 500 + 5\cos 0.1\,t \ [°c]$$

As it was discussed in Section 3, control input of air mass flow rate into intake manifold u_1 generated in Eq. (24) will be used for tracking reference signal x_{2r}, command mass flow rate of fuel u_2 calculated according to Eq. (33) regulates the virtual output corresponding to AFR reference signal y_r and spark angle u_3 based on Eq. (45) or Eq. (57) is assigned to the task of controlling catalyst temperature according to reference signal x_{4r}. Parameters K_1 and ω_0 corresponding to estimated catalyst temperature dynamic Eq. (47) are respectively equal to $K_1 = 0.9614$ and $\omega_o = 0.0133$. The response of closed-loop system considering the aforementioned configurations is described in Figures 2-4.

It can be observed from Figure 2 that the DCTCS algorithm has been successful in guiding the closed-loop system trajectory to time-varying reference signals despite the presence of sector-bounded modeling uncertainty and nonlinear dynamical effects. As it was discussed, tracking of crank-shaft velocity reference is conducted by adjusting air mass flow rate depicted in Figure 3. Then, fuel mass flow rate is set such that tracking of assigned AFR reference signal is ensured. In this configuration, reference AFR is assigned such that closed-loop system response resides in the second switched mode (as expressed in Figure 4) indicating that $y(k) < 14.7$. In this switched mode, the dynamical system operates such that fuel intake rate is lower than stoichiometric ratio. Corresponding virtual reference for fuel mass flow rate generating this AFR is depicted in Figure 2.c. Finally, control of catalyst temperature is conducted based on spark angle. As the Toyota 2AZ-FE engine operates as cold start, simultaneous increase in in exhaust and catalyst temperature is observed in transient-state stage before settling into their respective steady-state stage values.

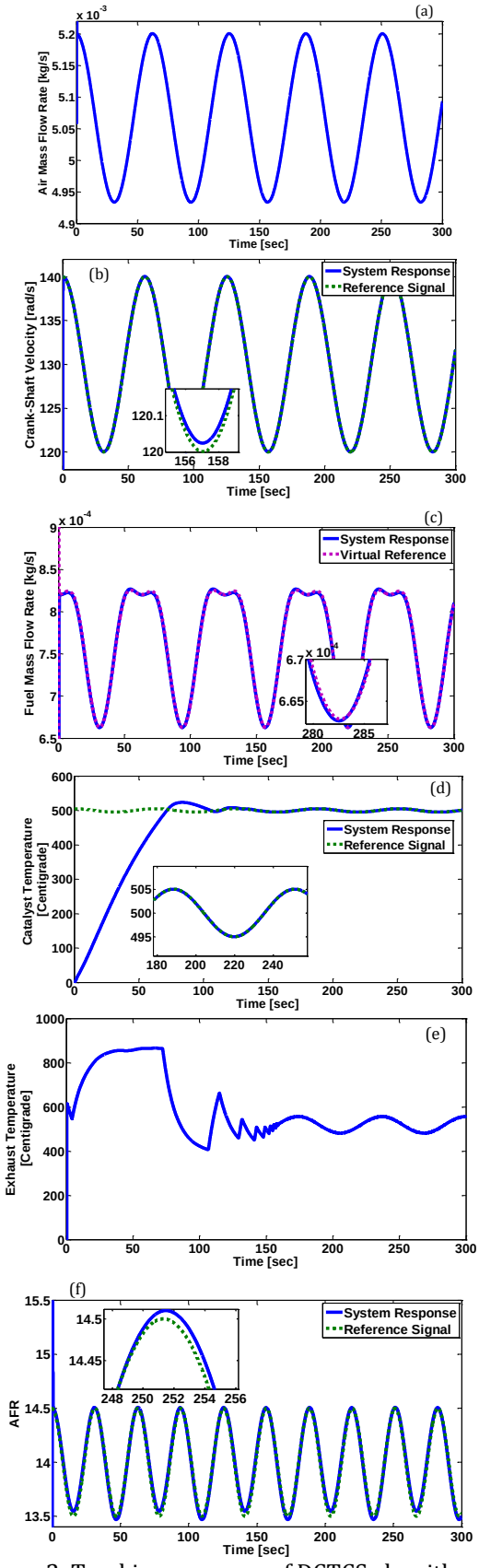

Figure 2: Tracking response of DCTCS algorithm for harmonic reference signals (a) Air mass in intake manifold (b) Crankshaft velocity (c) Fuel mass flow rate (d) Catalyst temperature (e) Exhaust combustion temperature (f) AFR

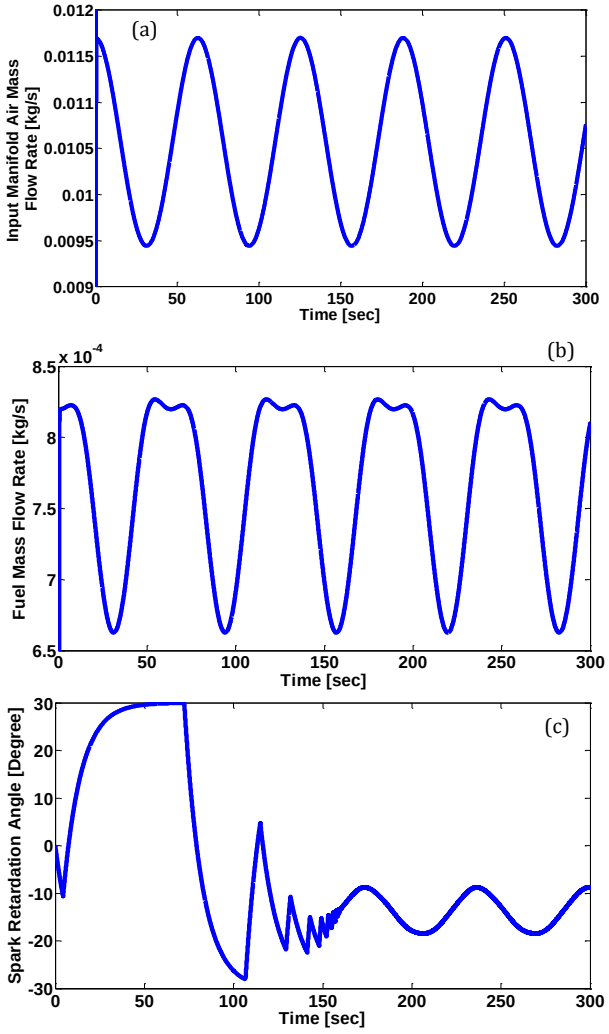

Figure 3: Control inputs of DCTCS algorithm for harmonic reference signals (a) Air mass flow rate into intake manifold (b) Command mass flow rate of fuel (c) Spark angle

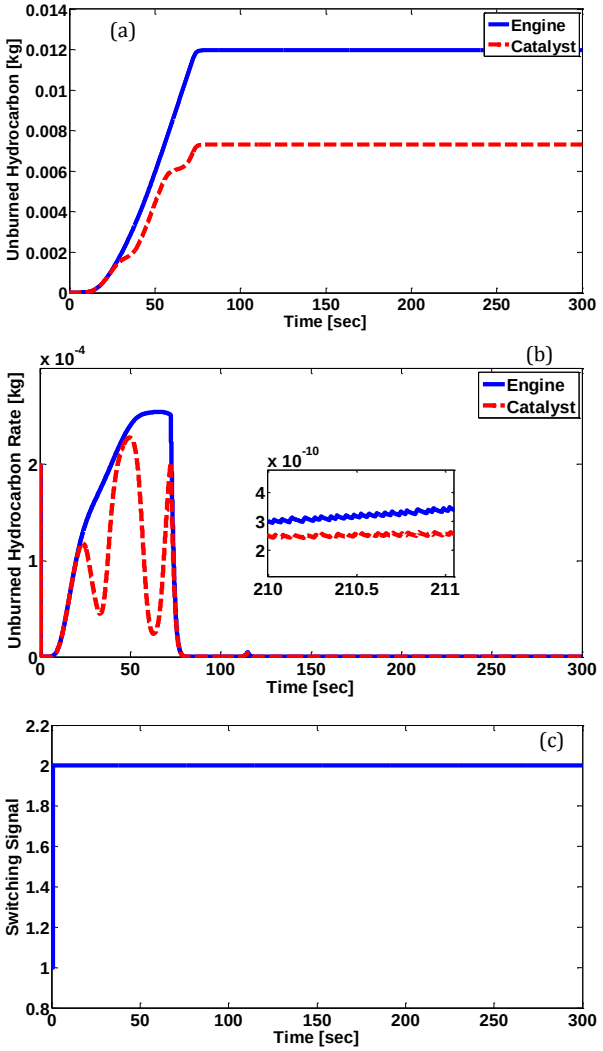

Figure 4: Pollution emission for engine and catalyst in the case of harmonic reference signal (a) Unburned hydrocarbon (b) Unburned hydrocarbon rate (c) Switching signal

This behavior is also observed in the associated graphs depicting unburned hydrocarbon in engine and catalyst. Naturally, unburned hydrocarbon in catalyst is a fraction of the value observed in engine, which indicates catalyst efficiency.

In Figures 5-7, the response of closed-loop system corresponding to rectangular wave reference signals is depicted. In this case, the AFR reference is set such that the dynamical system exhibits switched dynamic behavior with dwell-time of $30.0[s]$. Additionally, sampling period in this example is set to $T = 0.02[s]$ which is easily attainable by conventional devices, indicating feasibility of DCTCS using inexpensive hardware. However, it also has to be noted that increased sampling rate will result in higher tracking error in presence of modeling uncertainty. Due to discontinuities in assigned reference signals, multiple transient-state stages are observed corresponding to this mode of operation at discontinuous reference instants.

It can be observed from Figure 5 that the response of closed-loop system retains its boundedness at these periods as well before converging to associated sliding sets in steady-state stages. Control inputs depicted in Figure 6 generating the described pulse-width like motion resides in admissible region according to feasible operating constraints. From Figure 7, it is observed that the Toyota 2AZ-FE engine exhibits switched dynamic behavior in this configurations, which should be considered in construction of control model as described in Section 3.3 in order to ensure robust stability of closed-loop algorithms in all potential modes of switched dynamics configurations.

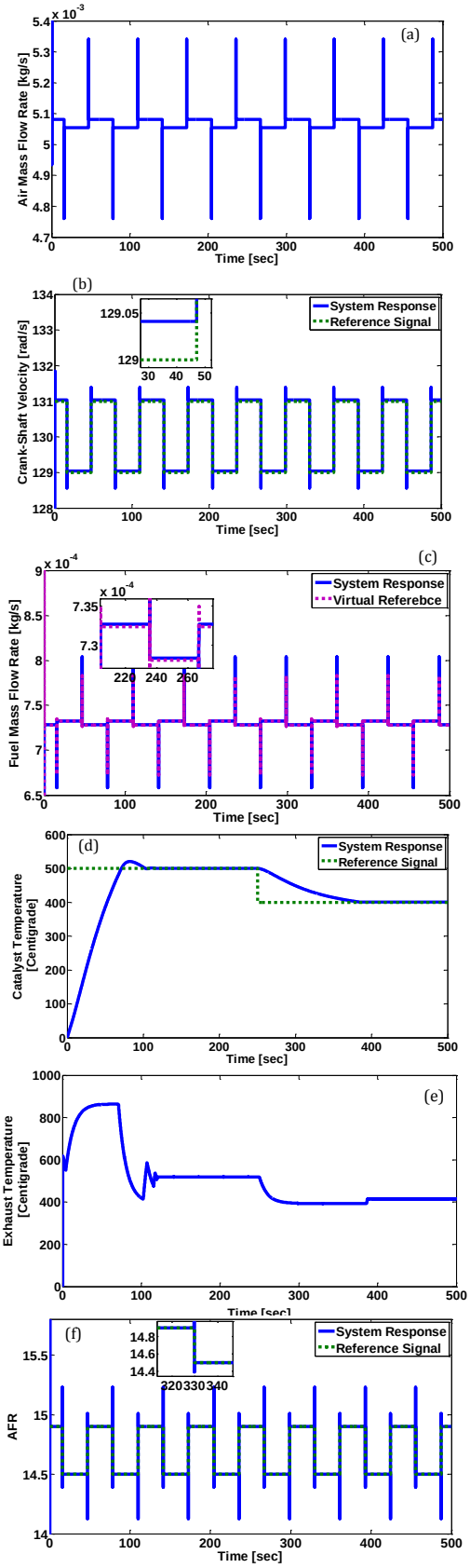

Figure 5: Tracking response of DCTCS algorithm for rectangular wave reference signals (a) Air mass in intake manifold (b) Crankshaft velocity (c) Fuel mass flow rate (d) Catalyst temperature (e) Exhaust combustion temperature (f) AFR

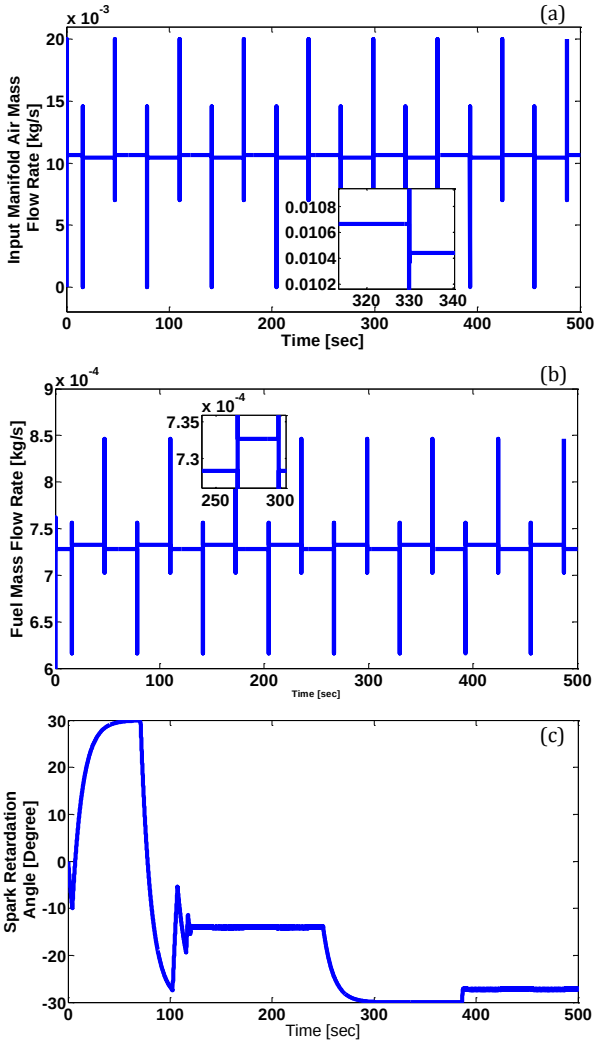

Figure 6: Control inputs of DCTCS algorithm for rectangular wave reference signals (a) Air mass flow rate into intake manifold (b) Command mass flow rate of fuel (c) Spark angle

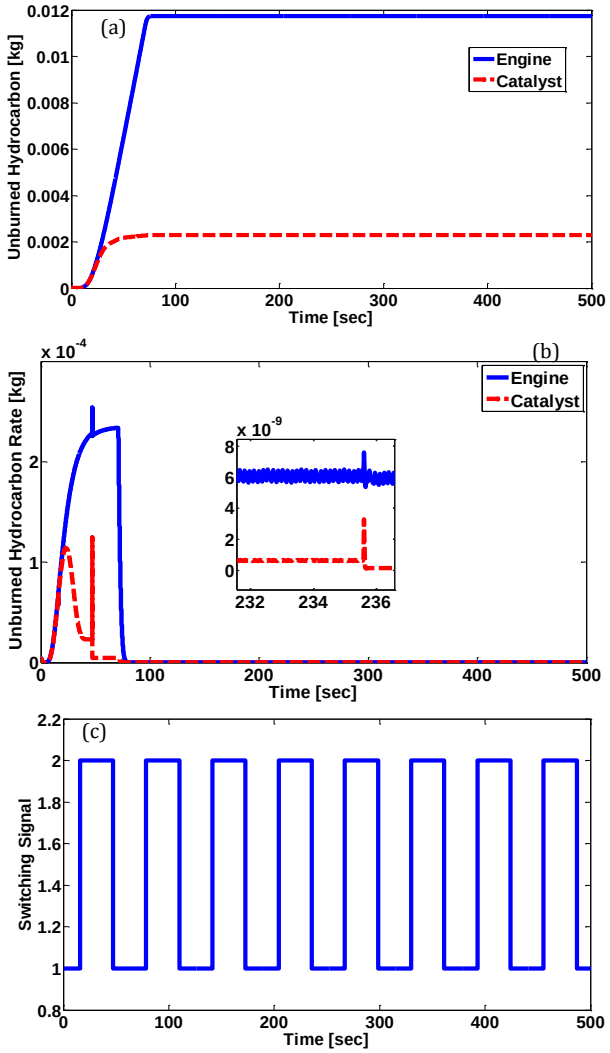

Figure 7: Pollution analysis for engine and catalyst in the case of rectangular wave reference signal (a) Unburned hydrocarbon (b) Unburned hydrocarbon rate (c) Switching signal

5) Conclusions

In this study, a new sliding control algorithm was obtained for stabilization of automotive systems employing Toyota 2AZ-FE cold start engine. The problems of control of crank-shaft velocity, AFR and catalyst temperature have been considered which constitute three distinct stages of construction of control model within a single control loop iterated at each sample. In all stages, nonlinear dynamic effects in the presence of modeling uncertainty are considered. Additionally, the effects of switching signal in stabilization of catalyst temperature are investigated. The proposed control algorithm is based on a DSMC model which does not result in high-frequency chattering effects since generated control inputs are not directly dependent on switching functions. Notable innovations in the proposed control algorithm constitute of model-based AFR control, a new control algorithm for tracking problem corresponding to catalyst temperature considering an additional virtual exponential input which is used in calculation of spark angle and a safe-mode control model ensuring that inputs generated for control of catalyst temperature are feasible regardless of the value of the aforementioned virtual output. Control tasks in all stages are conducted using the proposed DSMC algorithm which ensures stabilization of closed-loop system considering nonlinear dynamic effects, various modes of modeling uncertainty and multiple switched dynamics configurations. Numerical simulations used for illustration of control algorithm highlight the attained achievements.

List of Symbols

$\mathbf{x_1}$	Air mass in intake manifold
$\mathbf{x_2}$	Crankshaft velocity
$\mathbf{x_3}$	Fuel mass flow rate
$\mathbf{x_4}$	Catalyst temperature
$\mathbf{x_5}$	Exhaust combustion temperature
$\underline{\mathbf{x}}$	Continuous states vector
$\mathbf{u_1}$	Air mass flow rate into intake manifold
$\mathbf{u_2}$	Command mass flow rate of fuel
$\mathbf{u_3}$	Spark angle
$\underline{\mathbf{u}}$	Inputs vector
$\mathbf{f_i}$	Dynamical function describing governing dynamics of subsystem i corresponding to state x_i
$\underline{\mathbf{f_j}}$	Switched dynamical functions between inputs and states
$\mathbf{j}$	Switching index corresponding to stoichiometric ratio
$\mathbf{p_{i,j}}$	Engine parameters corresponding to individual dynamical functions
$\underline{\mathbf{\Phi}}$	Engine parameters vector
$\mathbf{\Phi_U}$	Uncertainty space for engine parameters vector
$\mathbf{g}(\underline{\mathbf{x}})$	Nonlinear dynamical functions
$\mathbf{u_3^*}$	A virtual control input corresponding to spark angle
$\mathbf{s_1}$	Sliding function corresponding to crankshaft velocity
$\mathbf{s_2}$	Sliding function corresponding to AFR
$\mathbf{s_3}$	Sliding function corresponding to catalyst temperature
$\boldsymbol{\lambda_i}$	Sliding function design parameter for s_i
$\mathbf{V_i}$	Lyapunov function corresponding to s_i
$\mathbf{T}$	Sampling period
$\mathbf{x_{ir}}$	Reference signal for state x_i
$\tilde{\mathbf{x}}_\mathbf{i}$	Tracking error of state x_i with

	respect to x_{ir}
$\boldsymbol{\xi_1[k,\Phi]}$	Dynamical variations term corresponding to $s_1(k+1)$
$\mathbf{b_i}$	Discrete-time input multiplier for s_1
$\mathbf{Sup}[\ ]_{\Phi_U}$	Supremum of bracketed term over uncertainty space $\boldsymbol{\Phi_U}$
$\mathbf{Inf}[\ ]_{\Phi_U}$	Infimum of bracketed term over uncertainty space $\boldsymbol{\Phi_U}$
$\mathbf{y}$	Output assigned to AFR value in construction of control scheme
$\boldsymbol{\alpha_i}$	Input bounds proximity factor for u_i
$\boldsymbol{\rho_i}$	Sliding layer width corresponding to s_i
$\mathbf{q_2^{(H)}}$	Upper input bound for u_2
$\mathbf{q_2^{(L)}}$	Lower input bound for u_2
$\mathbf{h_j(k,\Phi)}$	Dynamical terms used for expression of $x_{4j}(k)$
$\boldsymbol{\sigma_j(k,\Phi)}$	Control input gain for virtual input $u_3^*(k-1,j)$
$\boldsymbol{\mu}$	Finite-time convergence factor for $s_{3,j}(k)$
$\mathbf{N}$	Number of samples required for convergence of $s_{3,j}(k)$ to sliding set
$\boldsymbol{\mathcal{L}}$	Transfer function
$\mathbf{K_1, \omega_0}$	Parameters used for describing exhaust temperature dynamics in safe control mode
$\boldsymbol{\eta(k,\Phi)}$	Dynamical terms used for expressing $x_5(k)$
$\boldsymbol{\sigma_5(k,\Phi)}$	Input gains terms for u_3 in safe control mode

References

[1] C. Khajorntraidet, K. Ito, Simple adaptive air-fuel ratio control of a port injection SI engine with a cylinder pressure sensor, Control Theory and Technology, Vol. 13, No. 2, pp. 141–150, 2015

[2] C. Zhang, Y. Zhang, C. Chai, M. Zhou, Terminal sliding mode control of rail pressure for gasoline direct injection engines, Control Theory and Technology, Vol. 17, No. 2, pp. 183–189, 2019

[3] M. Hirata, S. Ishizuki, M. Suzuki, Two-degree-of-freedom H-infinity control of combustion in diesel engine using a discrete dynamics model, Control Theory and Technology, Vol. 15, No. 2, pp. 109–116, 2017

[4] W. Jiang, T. Shen, Nonlinear observer-based control design and experimental validation for gasoline engines with EGR, Control Theory and Technology, Vol. 17, No. 3, pp. 216–227, 2019

[5] Tabatabaei Oreh, S.H. Hamed, R. Kazemi, S. Azadi, A sliding-mode controller for directional control of articulated heavy vehicles, Proceedings of the Institution of Mechanical Engineers, Part D: Journal of Automobile Engineering, Vol. 228, No. 3, pp. 245–262, 2014.

[6] A. Abu Alqumsan, S. Khoo, M. Norton, Multi-surface sliding mode control of continuum robots with mismatched uncertainties, Meccanica, Vol. 54, No. 14, pp. 2307–2316, 2019

[7] H. Khajehsaeid, B. Esmaeili, R. Soleymani, A. Delkhosh. Adaptive back stepping fast terminal sliding mode control of robot manipulators actuated by pneumatic artificial muscles: continuum modelling, dynamic formulation and controller design. Meccanica, Vol. 54, No. 8, pp. 1203–1217, 2019

[8] S. Nüesch, P. Gorzelic, L. Jiang, J. Sterniak, A.G. Stefanopoulou, Accounting for combustion mode switch dynamics and fuel penalties in drive cycle fuel economy, International Journal of Engine Research, Vol. 17, No. 4, pp. 436–450, 2016

[9] M.R. Homaeinezhad, S. Yaqubi, F. Fotoohinia, FEA based discrete-time sliding mode control of uncertain continuum mechanics MIMO vibrational systems, Journal of Sound and Vibration, Vol. 460, pp. 114902, 2019

[10] M.R. Homaeinezhad, S. Yaqubi, Discrete-time sliding-surface based control of parametrically uncertain nonlinear systems with unknown time-delay and inaccessible switching mode detection, International Journal of Control, Vol. 94, No. 3, pp. 623-642, 2019

[11] M.R. Homaeinezhad, S. Yaqubi, H.M. Gholyan, Control of MIMO mechanical systems interacting with actuators through viscoelastic linkages. Mechanism and Machine Theory, Vol. 147, pp. 103763, 2020

[12] J. Zhang, L. Liu, X. Li, W. Li, Chattering-Free Sliding Mode Control for Diesel Engine Air Path System with Actuator Faults, IFAC-PapersOnLine, Vol. 51, No. 31, pp. 429–434, 2018

[13] Y. Q. Zhang, Y. S. Zhao, J. Yang, L. P. Chen. A dynamic sliding-mode controller with fuzzy adaptive tuning for an active suspension system. Proceedings of the Institution of Mechanical Engineers, Part D: Journal of Automobile Engineering, Vol. 221, No. 4, pp. 417–428, 2007

[14] Y. Yamasaki, R. Ikemura, M.Takahashi, S. Kaneko, A. Uemichi, Multiple-input multiple-output control of diesel combustion using a control-oriented model, International Journal of Engine Research, Vol. 20, No. 10, pp. 1005–

1016, 2019
[15] S. Pan, J.K. Hedrick, Tracking Controller Design for MIMO Nonlinear Systems with Application to Automotive Cold Start Emission Reduction, Journal of Dynamic Systems, Measurement and Control, Transactions of the ASME, Vol. 137, No.10, pp. 1–12, 2015
[16] M.R. Homaeinezhad, A. Shahhosseini, High-performance modeling and discrete-time sliding mode control of uncertain non-commensurate linear time invariant MIMO fractional order dynamic systems, Communications in Nonlinear Science and Numerical Simulation, Vol. 84, pp. 105200, 2020
[17] X. Su, X. Liu, P. Shi, R. Yang, Sliding Mode Control of Discrete-Time Switched Systems with Repeated Scalar Nonlinearities, IEEE Transactions on Automatic Control, Vol. 62, No. 9, pp. 6406-6410, 2016
[18] B. Bandyopadhyay, V.K. Thakar, Discrete time output feedback sliding mode control for nonlinear MIMO system: a stepper motor case, International Journal of Systems Science, Vol. 39, No. 1, pp. 89–104, 2008
[19] M.R. Amini, M. Shahbakhti, S. Pan, Adaptive discrete second-order sliding mode control with application to nonlinear automotive systems. Journal of Dynamic Systems, Measurement, and Control, Vol. 140, No. 12, 2018
[20] M.R. Amini, M. Shahbakhti, S. Pan, J.K. Hedrick, Bridging the gap between designed and implemented controllers via adaptive robust discrete sliding mode control, Control Engineering Practice, Vol. 59, pp. 1-15, 2017
[21] K. Edelberg, S. Pan, J.K. Hedrick, Design of automotive control systems robust to hardware imprecision, In Dynamic Systems and Control Conference, American Society of Mechanical Engineers, Vol. 56123, p. V001T12A002, 2013
[22] M. Amini, M. Shahbakhti, J.K. Hedrick. Discrete sliding controller design with robustness to implementation imprecisions via online uncertainty prediction, In 2016 American Control Conference (ACC), IEEE, pp. 6537-6542, 2016
[23] M.R. Amini, M. Shahbakhti, S. Pan, J.K. Hedrick, Handling model and implementation uncertainties via an adaptive discrete sliding mode controller design, In Dynamic Systems and Control Conference, American Society of Mechanical Engineers, Vol. 50701, pp. V002T28A001, 2016
[24] P.R. Sanketi, J.C. Zavala, J.K. Hedrick, M. Wilcutts and T. Kaga, A Simplified Catalytic Converter Model for Automotive Coldstart Applications with Adaptive Parameter Fitting, Int. Symp, on Advanced Vehicle Control, Vol. 8, pp, 62-65, 2006.
[25] P.R. Sanketi, Coldstart Modeling and Optimal Control Design for Automotive SI Engines, Ph.D. Dissertation, UC Berkeley, 2009.

فصلنامهٔ علمی تحقیقات موتور

تارنمای فصلنامه: www.engineresearch.ir

DOI:10.22034/ER.2022.697905

طراحی کنترل کننده غیرخطی دیجیتال برای فرایند گرم شدن واکنشگر شیمیایی یک موتور اشتعال جرقه ای

محمدرضا همایی‌نژاد [۱*]، صادق یعقوبی [۲]، وحید خرمی راد [۳]

[۱] دانشکده مهندسی مکانیک دانشگاه صنعتی خواجه نصیرالدین طوسی، ایران، mrhomaeinezhad@kntu.ac.ir

[۲] دانشکده مهندسی مکانیک دانشگاه صنعتی خواجه نصیرالدین طوسی، ایران، sadeq.yaqubi7@gmail.com

[۳] دانشکده مهندسی مکانیک دانشگاه صنعتی خواجه نصیرالدین طوسی، ایران، v.khorrami@email.kntu.ac.ir

[*] نویسندهٔ مسئول

چکیده

این مقاله، روش جدیدی را برای کنترل مد لغزشی گسسته، مبتنی بر مدل، برای استارت سرد یک موتور اشتعال جرقه‌ای با در نظر گرفتن اثرات دینامیک غیرخطی، عدم قطعیت مدل‌سازی و پیکربندی‌های سوئیچ چندگانه دینامیک را ارایه می‌دهد. الگوریتم کنترل با مساله تثبیت و ردیابی سرعت میل لنگ، نسبت هوا به سوخت و دمای کاتالیزور در حالت استارت سرد سروکار دارد. برای این منظور، یک تابع لغزش منحصر به فرد به هر مساله ردیابی اختصاص داده شده که متعاقباً در ساخت تابع لیاپانوف مرتبط استفاده می شود. سرعت میل لنگ با استفاده از نرخ جریان جرم هوا در راهگاه ورودی با در نظر گرفتن معادلات دینامیکی مرتبط که جریان جرم هوا را توصیف می‌کنند، تنظیم می‌شود. برای اطمینان از کنترل دقیق نسبت هوا به سوخت، مدل کنترل لغزشی با در نظر گرفتن نرخ جریان جرم هوا محاسبه است که منجر به عبارات غیر خطی می شود که متعاقباً در محاسبه نرخ جریان جرم سوخت مناسب به کار می روند. تثبیت دمای کاتالیزور از طریق تعریف ورودی کنترلی مجازی مربوط به زاویه جرقه انجام می شود. از آنجایی که دمای کاتالیزور با استفاده از عبارات ریاضی لگاریتمی توصیف می‌شود، مراحل اضافی باید برای اطمینان از امکان‌سنجی الگوریتم کنترل در شرایط عملیاتی مختلف در نظر گرفته شود. کنترل طراحی شده به صورت عددی در مدل ریاضی معتبر موتور تویوتا 2AZ-FE اعمال شد تا کارایی و دقت عملکرد بازخورد را ارائه دهد.

اطلاعات مقاله

تاریخچهٔ مقاله:

دریافت: ۲ اردیبهشت ۱۴۰۱

پذیرش: ۲۵ خرداد ۱۴۰۱

کلیدواژه‌ها:

کنترل دیجیتال موتور

فرآیند سوئیچینگ

موتور اشتعال جرقه ای

کنترل مد لغزشی

کنترل مقاوم